SELF-ADAPTIVE GAP/FRICTION ELEMENT IN MSC/NASTRAN

Sang H. Lee and T. L. Lin[1]
The MacNeal-Schwendler Corporation
815 Colorado Blvd., Los Angeles, CA 90041

Abstract

One of the major areas in nonlinear analysis that poses difficulties in convergence is the application of GAP elements. This has been particularly true when friction is involved. Numerical difficulty is inherent in nature for the penalty method which is employed in the MSC/NASTRAN GAP element. Furthermore, the GAP element simulates a point-to-point contact, and is often used to simulate surface contact problems. Deficiencies of the penalty GAP element are coped with by implementing an adaptive GAP element in Version 67 of MSC/NASTRAN. The adaptability is based on the subincremental scheme with a capability to update the stiffness at the appropriate time, bisect when the increment is excessive, and adjust penalty stiffnesses to the proper values in concert with the nonlinear and dynamic environment. In addition, the kinetic friction effect (different from the static friction) is introduced to simulate the physics more accurately by distinguishing stick-slip forces.

I. INTRODUCTION

Contact problems are very common in engineering practice. The GAP element simulates a unidirectional point-to-point contact using the bulk data CGAP and PGAP. The GAP element is one of the major areas that pose difficulties to the convergence of the iterative process, particularly when friction is involved. The penalty method is used to simulate the rigidity between two degrees of freedom by adding a large value to the stiffness so that the two have approximately the same displacements. Penalty values are introduced to avoid penetration and to enforce the sticking condition (static friction) between two contact points. Difficulties (or inaccuracies) arise when the penalty values are not properly chosen. The success of this method is highly dependent on the user's choice of penalty values and requires a compromise between accuracy and ease of convergence.

The Lagrange multiplier method has been used by researchers [1-3] in contact problems. The method enforces the constraints exactly. However, it also poses some difficulties. The main drawbacks of the Lagrange multiplier method are: (1) the problem size increases by Lagrange multiplier variables and (2) the stiffness matrix has zero diagonal terms, and requires pivoting and resequencing. Some variations of the Lagrange multiplier method have been proposed

[1]former employee, currently at Cray Research

[4-6] to mitigate the deficiencies. Another school of thought for the dilemma is to alleviate the difficulties by implementing the capability for the penalty method to choose or adjust to proper penalty values and control the numerical stability and the accuracy [7-8]. Although the constraint is not enforced exactly, the effectiveness of the penalty method lies in preserving the size and the bandwidth of the stiffness matrix. MSC/NASTRAN employs this approach in the adaptive GAP element implemented in Version 67.

II. BASIC CONSIDERATIONS FOR PENALTY GAP ELEMENT

The GAP element changes its status when the load is applied. Consider the internal forces of a GAP element with an isotropic friction. Force components in the GAP element are the axial compressive force (F_x) and the friction forces in lateral directions (F_y and F_z) in terms of displacements (u, v, w) in the element coordinate system. These internal forces can be computed based on the GAP status as follows:

- When the GAP is open (no contact, no lateral stiffness),

$$F_x = K_b u \leq 0. \qquad \text{and} \qquad F_y = F_z = 0. \tag{1}$$

  where K_b is an arbitrary open stiffness.

- When the GAP is closed and sliding (no friction),

$$F_x = K_a u > 0. \qquad \text{and} \qquad F_y = F_z = 0 \tag{2}$$

  where K_a is the penalty value for the closed stiffness.

- When the GAP is closed and sticking (static friction),

$$F_y^2 + F_z^2 \leq (\mu_s F_x)^2 \tag{3}$$

  where $F_x = K_a u$, $F_y = K_t v$, and $F_z = K_t w$ using a static coefficient of friction (μ_s) and the transverse shear stiffness (K_t).

- When the GAP is closed and slipping (kinetic friction),

$$F_y^2 + F_z^2 > (\mu_k F_x)^2 \tag{4}$$

  where

$$F_x = K_a u, \quad F_y = \frac{v \mu_k F_x}{\sqrt{v^2 + w^2}}, \text{ and } F_z = \frac{w \mu_k F_x}{\sqrt{v^2 + w^2}}$$

The (6 x 6) element stiffness matrix can be formed as

$$[K] = \begin{bmatrix} \tilde{K} & -\tilde{K} \\ -\tilde{K} & \tilde{K} \end{bmatrix} \qquad \text{with} \qquad \tilde{K} = \frac{\partial\{F\}}{\partial\{u\}}$$

The stiffness components are derived for each GAP status as follows:

- When the GAP is open,

$$\tilde{K} = \begin{bmatrix} K_b & 0. & 0. \\ & 0. & 0. \\ sym. & & 0. \end{bmatrix} \tag{5}$$

- When the GAP is closed and sliding,

$$\tilde{K} = \begin{bmatrix} K_a & 0. & 0. \\ & 0. & 0. \\ sym. & & 0. \end{bmatrix} \tag{6}$$

- When the GAP is closed and sticking,

$$\tilde{K} = \begin{bmatrix} K_a & 0. & 0. \\ & K_t & 0. \\ sym. & & K_t \end{bmatrix} \tag{7}$$

- When the GAP is closed and slipping,

$$\tilde{K} = \frac{K_a}{(v^2+w^2)^{3/2}} \begin{bmatrix} (v^2+w^2)^{3/2} & 0. & 0. \\ \mu_k v(v^2+w^2) & \mu_k uw^2 & -\mu_k uvw \\ \mu_k w(v^2+w^2) & -\mu_k uvw & \mu_k uv^2 \end{bmatrix} \tag{8}$$

It is noted that the slipping due to friction introduces an unsymmetric stiffness matrix.

There are some inherent difficulties involved in the penalty GAP element. Since the Newton's method is sensitive to abrupt changes in stiffness during iterations, it could cause a divergent or oscillatory solution when the GAP changes its status. The timing of the stiffness update is crucial to the convergence, which necessitates an adaptive stiffness update criterion based on the GAP status. If the GAP status undergoes two or more consecutive changes, adaptive stiffness update alone cannot stabilize the solution and a bisection strategy becomes necessary.

The behavior of the GAP element with friction is path-dependent in a manner similar to plasticity. The lateral forces due to friction should be considered for equilibrium. If the internal forces in the GAP elements are computed in a single step for the change in displacements, the accuracy deteriorates when the increment produces large changes in displacements with friction. In order to trace the path-dependent solution, the subincremental scheme within an incremental load step is desirable [9].

Optimal penalty values (K_a and K_t) are difficult to assess. Furthermore, they have to be updated adaptively during the deformation, since the stiffness of the adjacent structure changes during the incremental process. It becomes necessary to adjust penalty values adaptively by the program throughout the analysis.

III. USER INTERFACE FOR GAP ELEMENT

Connectivity is specified in the bulk data entries CGAP as shown below:

1	2	3	4	5	6	7	8	9	10
CGAP	EID	PID	GA	GB	X1,G0	X2	X3	CID	
CGAP	17	2	110	112				3	

Line GA-GB defines the GAP element x-axis as shown in Figure 1. If GA and GB are coincident in space, CID is used to define the element coordinate system. The orientation of the y and z axes is determined by G0 (or X1, X2, X3) defining the x-y plane. The element coordinate system does not rotate as a result of deflections. In other words, the element coordinate system is not updated even when the geometric nonlinearity is considered (LGDISP=1).

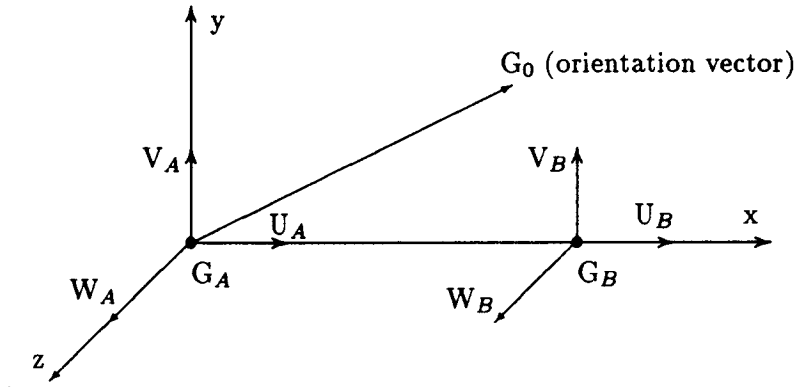

Figure 1. The Gap Element

The axial and lateral force-deflection curves of the GAP element are shown in Figures 2 and 3. Properties that characterize these curves are specified in the bulk data PGAP.

1	2	3	4	5	6	7	8	9	10
PGAP	PID	U_0	F_0	K_a	K_b	K_t	μ_1	μ_2	
PGAP	2	0.	0.	1.E6	1.E−2	1.E5	0.	0.	+PG

	TMAX	MAR	TRMIN						+PG
+PG	0.	100.	0.001						

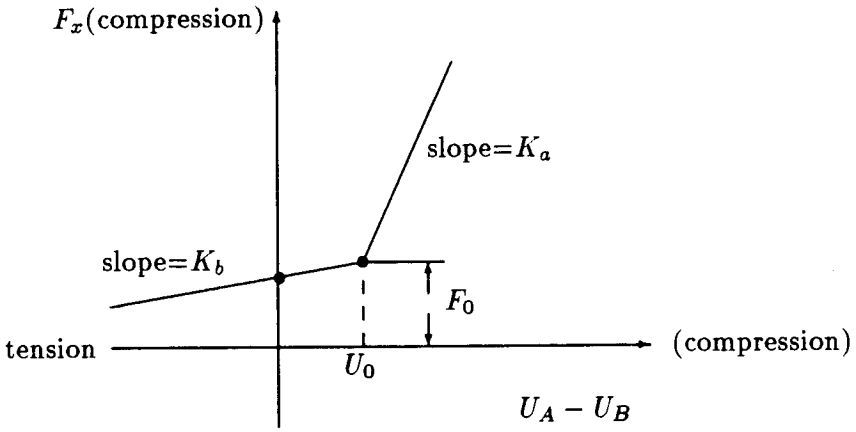

Figure 2. Gap Axial Force vs. Deflection
(slope K_a is used when $U_A - U_B \geq U_0$)

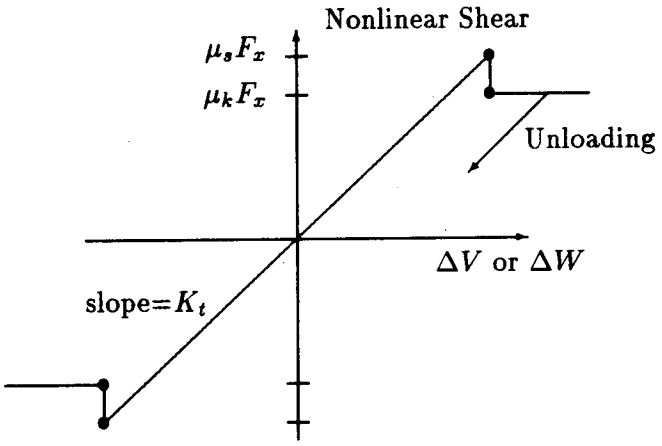

Figure 3. Gap Lateral Force vs. Deflection

The initial GAP opening is defined by u_0 (defaulted to 0), not by the separation distance. The preload is defined by F_o (defaulted to 0). Notice that positive values of force and displacement represent compression in the GAP element coordinates. If the GAP is closed ($u_A - u_B \geq u_o$), the axial stiffness (K_a) has a large value relative to the adjacent structure. When the GAP is open, there is a small open stiffness (K_b, which is defaulted to $10^{-8}K_a$) in the axial direction. For most contact problems, K_a should be chosen to be three orders of magnitude higher than the stiffness of the neighboring grid points. The factor may be reduced to facilitate convergence at the expense of the accuracy. A much larger K_a value may slow down convergence or cause divergence, while a much smaller K_a value may result in an inaccuracy.

The transverse shear stiffness K_t (defaulted to $0.1K_a$) is used when the friction is active upon contact. When the GAP is open, there is no transverse stiffness. When the GAP is closed and if there is friction, the GAP has the elastic stiffness (K_t) in the transverse direction until the lateral force exceeds the friction force and the slip starts to occur. If $K_t = 0$, the friction effect is ignored (equivalent to $\mu_1 = \mu_2 = 0$). The recommended range of the transverse stiffness value is $0.01K_a \leq K_t \leq K_a$.

When the adaptive GAP (default option) is used, μ_1 and μ_2 represent static and kinetic coefficients of friction μ_s and μ_k, respectively. If the nonadaptive GAP element is chosen, the anisotropic coefficients of friction (μ_y and μ_z) are the input for μ_1 and μ_2. Directions y and z are defined by the orientation vector in the CGAP entry, which corresponds to the GAP element coordinate system.

Penalty values (K_a and K_t) are adjusted adaptively if $TMAX > 0.0$. There are two kinds of GAP elements: adaptive GAP and nonadaptive GAP. If $TMAX \geq 0.0$, the adaptive GAP element is chosen. When $TMAX = 0.0$ (default option), penalty values will not be adjusted but other adaptive features will be active (the gap induced stiffness update, gap induced bisection, and subincremental process). The value of $TMAX = -1.0$ selects the nonadaptive (old) GAP element. The recommended allowable penetration TMAX is about 10% of the element thickness for plates and shells (or equivalent thickness for other elements) which are connected to the GAP element.

The maximum adjustment ratio MAR ($1 < MAR < 10^6$, defaulted to 100) is used only for penalty value adjustment of the adaptive GAP element. Upper and lower bounds of the adjusted penalty value are $MAR * K^0$ and K^0/MAR, respectively, where K^0 is the user-specified value for K_a or K_t. The parameter TRMIN is a fractional number ($0.0 \leq TRMIN \leq 1.0$, defaulted to 0.001), representing a lower bound for the allowable penetration. The lower bound for the allowable penetration is computed by $TRMIN * TMAX$. The penalty values are decreased if the penetration is below the lower bound.

GAP element output may be obtained by the STRESS ouput request in the Case Control Section. An example of the GAP output format is shown below:

ELETRO-MECHANICAL CLUTCH SEPTEMBER 5, 1990 MSC/NASTRAN 8/30/90 PAGE 66

DISPLACEMENT IN MM., FORCE IN NEWTON

SUBCASE 1

LOAD STEP = 2.00000E-01

STRESSES (FORCES) IN GAP ELEMENTS (CGAP)

ELEMENT	-FORCES IN ELEM SYSTEM-			-DISPLACEMENTS IN ELEM SYSTEM-					
ID	COMP-X	SHEAR-Y	SHEAR-Z	AXIAL-U	TOTAL-V	TOTAL-W	SLIP-V	SLIP-W	STATUS
31	1.2051E-06	0.0	0.0	1.2977E-02	-2.3891E-01	0.0	-2.3891E-01	0.0	SLIDE

The element forces and displacements are computed in the element coordinate system. Positive values of the axial force (F_x) and the axial displacement (U) represent compression. Lateral forces are computed for the frictional case, and printed as SHEAR-Y and SHEAR-Z. Lateral displacements in the y and z directions are printed under TOTAL-V, TOTAL-W (representing total lateral displacements) and SLIP-V, SLIP-W (representing translation of the slip center). When the GAP is open (regardless of friction) or sliding without friction, the total displacements (TOTAL-V, TOTAL-W) and the slip center displacements (SLIP-V, SLIP-W) have the same value. For the sticking or slipping cases with friction, the magnitude of the slip center translation (SLIP-V, SLIP-W) should be smaller than the magnitude of the total displacement. The last column of the output shows the GAP status (available in V67): OPEN, SLIDE, STICK or SLIP.

IV. THEORETICAL BASIS FOR FRICTIONAL BEHAVIOR

According to the Coulomb friction law, the reaction force due to friction is proportional to the normal force (F_N). Slipping does not occur as long as the external force exerted in the lateral direction (F_T) is smaller than the friction force, i.e.,

$$F_T \leq \mu_s F_N$$

where μ_s is the static coefficient of friction. Slipping starts when the external lateral force exceeds the static friction force. The friction force is reduced to the kinetic friction force ($\mu_k F_N$) during the slip, since $\mu_k < \mu_s$ in general.

In order to simulate the stick-slip behavior of the current GAP element, the frictional yield function is formed as follows:

$$f = \sqrt{F_y^2 + F_z^2} - \mu_s F_x \tag{9}$$

with

$$\begin{Bmatrix} F_y \\ F_z \end{Bmatrix} = K_t \begin{Bmatrix} v - v_s \\ w - w_s \end{Bmatrix} \tag{10}$$

where K_t is an elastic stiffness (representing a penalty value) during sticking, and (v_s, w_s) represents a translation of the slip center in the y-z plane. The GAP is **sticking**, if $f < 0$.

When the GAP starts to **slip** ($f \geq 0$), the lateral displacement can be decomposed into two parts: recoverable part (sticking, denoted by superscript st) and irrecoverable part (slipping, denoted by superscript sl); i.e.,

$$\left\{ \begin{array}{c} \Delta v \\ \Delta w \end{array} \right\} = \left\{ \begin{array}{c} \Delta v^{st} \\ \Delta w^{st} \end{array} \right\} + \left\{ \begin{array}{c} \Delta v^{sl} \\ \Delta w^{sl} \end{array} \right\} \tag{11}$$

Slipping is similar to plasticity [9]. Adopting the associated flow rule, the slip displacements can be defined in terms of the equivalent slip increment ($\Delta\bar{\gamma}^{sl}$) by

$$\left\{ \begin{array}{c} \Delta v^{sl} \\ \Delta w^{sl} \end{array} \right\} = \Delta\bar{\gamma}^{sl} \frac{1}{\mu_k F_x} \left\{ \begin{array}{c} F_y \\ F_z \end{array} \right\} \tag{12}$$

where

$$\mu_k F_x = \sqrt{F_y^2 + F_z^2}$$

and

$$\Delta\bar{\gamma}^{sl} = \sqrt{\Delta v^{sl\,2} + \Delta w^{sl\,2}}$$

Notice that slipping occurs along the direction normal to the slip locus, where (F_y, F_z) represent the forces in the normal direction to the slip locus.

The slip yield surface is kept up-to-date by updating slip forces and the slip center (similar to kinematic hardening). Substituting Eqs. (11) and (12) into (10), we obtain

$$\left\{ \begin{array}{c} F_y \\ F_z \end{array} \right\} = \frac{1}{1 + \Delta\bar{\gamma}^{sl} \frac{K_t}{\mu_k F_x}} \left\{ \begin{array}{c} F_y^{trial} \\ F_z^{trial} \end{array} \right\} \tag{13}$$

where

$$\left\{ \begin{array}{c} F_y^{trial} \\ F_z^{trial} \end{array} \right\} = K_t \left\{ \begin{array}{c} \Delta v \\ \Delta w \end{array} \right\}$$

Substituting Eq. (13) into Eq. (9) with $f = 0$, we can express $\Delta\bar{\gamma}^{sl}$ as below:

$$\Delta\bar{\gamma}^{sl} = \frac{\sqrt{F_y^{trial\,2} + F_z^{trial\,2}} - \mu_k F_x}{K_t} \tag{14}$$

Combining Eq. (13) and (14), the final form of Eq. (13) becomes

$$\left\{ \begin{array}{c} F_y \\ F_z \end{array} \right\} = \frac{\mu_k F_x}{\sqrt{F_y^{trial\,2} + F_z^{trial\,2}}} \left\{ \begin{array}{c} F_y^{trial} \\ F_z^{trial} \end{array} \right\} \tag{15}$$

The slip center must be updated accordingly using Eq. (12), (14) and (15):

$$\left\{ \begin{array}{c} v_s \\ w_s \end{array} \right\} = \left\{ \begin{array}{c} v \\ w \end{array} \right\} - \frac{1}{K_t} \left\{ \begin{array}{c} F_y \\ F_z \end{array} \right\} \tag{16}$$

V. SUBINCREMENTAL ALGORITHM FOR STIFFNESS UPDATE AND BISECTION

In the absence of friction, the GAP element may change its status from open to sliding and vice versa. When friction is present, the status of the GAP element may change from open to stick (closed) and further to slip (closed), and vice versa. General principles adopted in the adaptive stiffness matrix update and bisection strategies induced by GAP elements are:

- Allow only one state change in any GAP element within each increment. Bisect the load or time step if the GAP undergoes two state changes (e.g., open to slip) in a single step.
- Update the stiffness matrix when stiffening is detected due to GAP status change (e.g., open to stick, or slip to stick).
- Subdivide the increment for the slip process [9].

In order to achieve the adaptability, it is necessary to use the subincremental approach within a global increment. Furthermore, slipping with friction is a path-dependent process. The subincremental scheme allows a more accurate solution to the path-dependent process.

Two major steps are required to implement the subincrement method. Let the displacement increment for the $i-$th iteration be defined as follows:

$$\left\{ \begin{array}{c} \Delta u \\ \Delta v \\ \Delta w \end{array} \right\} = \left\{ \begin{array}{c} u^i - u_n \\ v^i - v_n \\ w^i - w_n \end{array} \right\}$$

where n represents the previously converged step. The first step is to find the **open/close** boundary. Assume that the GAP closes from the opening state at the $i-$th iteration. The scale factor α $(0 \leq \alpha \leq 1)$ is used to determine the point at which the GAP starts to close as follows:

$$\alpha = \left\{ \begin{array}{lll} \frac{u_0 - u_n}{\Delta u} & if \quad u_n \leq u_0 \leq u^i & \text{(open} \rightarrow \text{closed)} \\ 0 & if \quad u_n \geq u_0 & \text{(closed} \rightarrow \text{closed)} \end{array} \right. \tag{17}$$

where u_0 represents the initial opening of the GAP element.

The second step is to find the **stick/slip** boundary. Assume that the GAP changes status from stick to slip at the $i-$th iteration. The scale factor β $(0 \leq \beta \leq 1)$ is used to determine the point where the GAP begins to slip. The frictional yield function should be satisfied $(f = 0)$ at the stick/slip boundary, i.e.,

$$\mu_s(F_x^n + \beta K_a \Delta u) = \sqrt{(F_y^n + \beta K_t \Delta v)^2 + (F_z^n + \beta K_t \Delta w)^2} \tag{18}$$

Eq. (18) can be rearranged to solve for β, resulting in a quadratic function of β.

$$a\beta^2 + 2b\beta + c = 0 \tag{19}$$

where

$$
\begin{aligned}
a &= (\mu_s K_a \Delta u)^2 - K_t^2(\Delta v^2 + \Delta w^2) \\
b &= \mu_s^2 F_x^n K_a \Delta u - K_t(F_y^n \Delta v + F_z^n \Delta w) \\
c &= \mu_s^2 F_x^{n2} - F_y^{n2} - F_z^{n2}
\end{aligned}
$$

where F_x^n, F_y^n and F_z^n represent GAP internal forces at the last converged solution. It can be shown that the quadratic equation is guaranteed to produce a real and positive root. Since the GAP is slipping at the $i-$th iteration,

$$f = \sqrt{F_y^{i2} + F_z^{i2}} - \mu_k F_x^i > 0 \tag{20}$$

Expanding Eq. (20) using the relation in Eq. (19), the following inequalities can be obtained:

$$a + 2b + c < 0 \qquad \text{and} \qquad b^2 - ac > \left(\frac{a-c}{2}\right)^2 \geq 0$$

These inequalities lead to a proper root

$$\beta = \frac{-b - \sqrt{b^2 - ac}}{a}$$

and for $a \simeq 0$

$$\beta = -\frac{c}{2b}$$

Once the initial slip point is found, the slip region should be subdivided into m subincrements ($1 < m \leq 10$). The number of subdivisions are determined adaptively by

$$m = INT(\frac{f^i}{0.5 * \mu_k * F_x}) + 1 \tag{21}$$

The displacement increment for each subincrement becomes

$$\begin{Bmatrix} \Delta u^m \\ \Delta v^m \\ \Delta w^m \end{Bmatrix} = \frac{1}{m}(1-\alpha)(1-\beta) \begin{Bmatrix} u^i - u_n \\ v^i - v_n \\ w^i - w_n \end{Bmatrix}$$

The GAP normal force (F_x) is gradually increased, and the radial return method is used to update the slip force in m subincrements. After the subincremental process, the element stiffness and the slip center are updated. The subincremental process is schematically described in Figure 4.

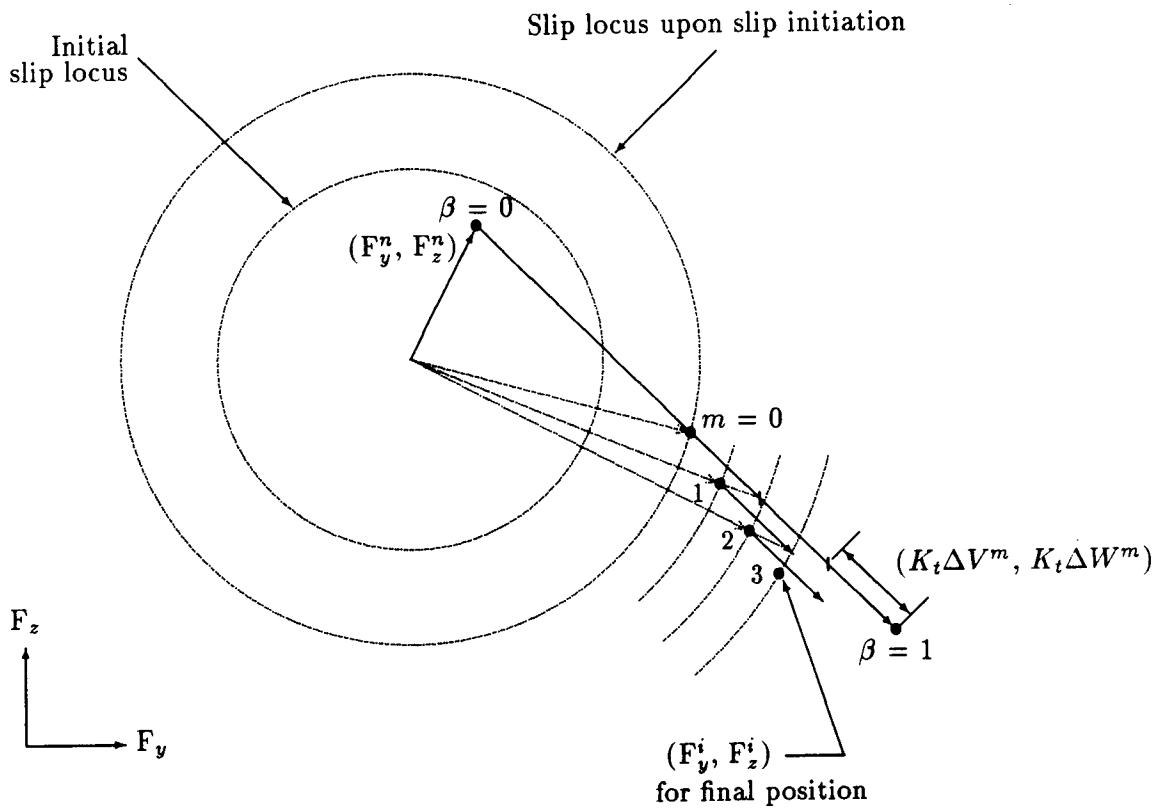

Figure 4. Schema for Subincremental Process ($m = 3$)

It is noted that the "slip to slip" case is catagorized into two groups. One is the slip in the same direction and the other is the slip in the opposite direction. The condition for the slip in the same direction can be determined by the dot product of the last converged friction force and the friction force increment:

$$[F_y^n(F_y^{trial} - F_y^n) + F_z^n(F_z^{trial} - F_z^n)] \geq 0$$

Slipping in the same direction is also signified by a double root of β at zero. If the slip occurs in the opposite direction, β has two roots with one being zero. In this case, the root at zero is discarded and the subincrement is processed from the slip locus at the opposite side signified by the nonzero β.

VI. ADAPTIVE ADJUSTMENT OF PENALTY VALUES

Penalty values are adaptively adjusted upon convergence for the next increment. If the penalty value is too small to produce an appreciable penetration, the accuracy of the solution

may not be acceptable. Then the penalty value (K_a) should be increased to reduce the penetration. On the other hand, numerical difficulties arise if the penalty values are set too high. It is highly desirable to reduce the penalty values in such cases.

The adaptive penalty value adjustment is designed to adjust penalty values automatically, if necessary, starting from the user-specified penalty values and the maximum allowable penetration (TMAX). If the GAP penetration exceeds the allowable value supplied by the user, penalty values (K_a and K_t) are increased, and vice versa if the penetration is smaller than the minimum allowable value ($TMAX * TRMIN$). The adjustments are made at converged points. It is necessary to introduce a stepping function in order to avoid thrashing [10]. The stepping function is designed such that the adjustment ratio is in powers of 10, i.e.,

$$K^{n+1} = f(R)K^n \tag{22}$$

where $f(R)$ is ..., 0.1, 1., 10, ... and n denotes the incremental step with

$$R = \frac{u - u_0}{TMAX} \qquad \text{if} \qquad u - u_0 > TMAX$$

or

$$R = \frac{u - u_0}{TMAX * TRMIN} \qquad \text{if} \qquad u - u_0 < TMAX * TRMIN$$

It is noted that two penalty values (K_a and K_t) are adjusted by the same ratio, starting from the user-specified initial values. Since the ratio of K_a to K_t constitutes the slip criterion, a disparity will occur between two consecutive solutions if K_a and K_t are adjusted independently. The ratio between two penalty values can be established logically. Assume that the lateral displacement under the sticking condition is ϵ when the GAP starts to slip. The slip condition requires that

$$\mu_k K_a(u - u_0) = K_t \epsilon$$

If it is desired to limit the lateral displacement under the sticking condition (ϵ) by the same magnitude as the normal penetration ($u - u_0$), the magnitude of shear stiffness K_t has to be related to K_a by

$$K_t \simeq \mu_k K_a \,. \tag{23}$$

If the user inputs $TMAX = 0$, the penalty value is fixed and the adjustment algorithm is not invoked. The penalty value adjustment is limited by an upper and lower bound defined by the user-specified maximum adjustment ratio (MAR), i.e.,

$$\frac{K^0}{MAR} \leq K \leq MAR * K^0 \tag{24}$$

where K^0 is the user-specified value for K_a or K_t. The global stiffness matrix is updated whenever the penalty values are adjusted.

VII. VERIFICATION and VALIDATION

BOUNCING MASS PROBLEM

A 4-lb weight is resting on a spring-supported platform which is initially compressed 4 inches in the position shown in Figure 5. The platform is released, and after moving 2 inches, the platform is halted by a stopper. The response of the weight is to be determined [11]. The spring modulus of the platform support is 10 lb/in.

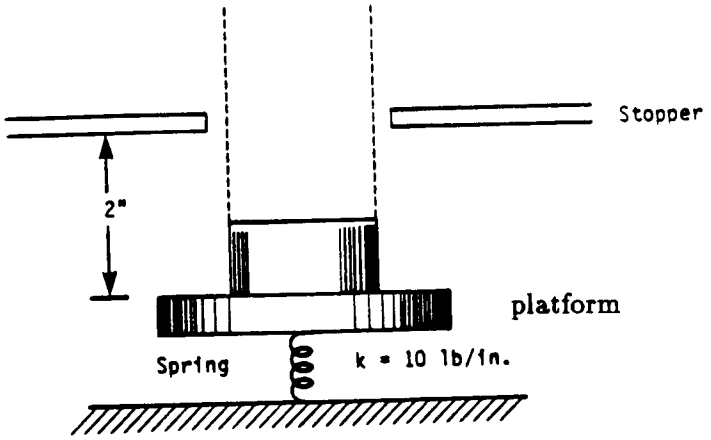

Figure 5. Physical Model

From the conservation of energy

$$\Delta V_e + \Delta V_g + \Delta T = 0. \tag{25}$$

The change in energy from the initial state when the platform is stopped is

$$\Delta V_e = \frac{1}{2}k(x_1^2 - x_0^2) = -60 \text{ lb-in}$$

$$\Delta V_g = mgh = 8 \text{ lb-in}$$

$$\Delta T = \frac{1}{2}m\dot{x}_0^2$$

from which the velocity of the mass at the time of departure from the platform can be obtained as

$$\dot{x}_0 = \sqrt{\frac{2}{m}(-\Delta V_e - \Delta V_g)} = 100.1798 \text{ in/sec.}$$

Up to this point, the motion of the mass is governed by the equation

$$m\ddot{x} + kx = -mg. \tag{26}$$

With the initial conditions $x_0 = -4$ in and $\dot{x}_0 = 0$ in/sec, the response of the mass is expressed as

$$x = (x_0 + \frac{mg}{k})\cos\omega_n t - \frac{mg}{k} \tag{27}$$

The elapsed time at the moment the platform hits the stopper may be obtained by solving the above equation for t with $x_1 = 2$ in, i.e.,

$$t_1 = \frac{1}{\omega_n} \cos^{-1} \left(\frac{x_1 + \frac{mg}{k}}{x_0 + \frac{mg}{k}} \right) = 0.0357 \text{ sec}$$

where $\omega_n = \sqrt{\frac{k}{m}} = 31.0644$ rad/sec. As the mass departs from the platform, the motion of the mass is described by

$$h = \dot{x}_0 t - \frac{1}{2} g t^2 \tag{28}$$

relative to the stopper. Elasped time when the mass reaches the peak is obtained as

$$t_2 = t_1 + \frac{\dot{x}_0}{g} = 0.0357 + 0.2595 = 0.2953 \text{ sec.}$$

The height of the mass at this moment is

$$h_{max} = \frac{\dot{x}_0^2}{2g} = 13.0 \text{ in}$$

from the stopper. The theory predicts that one full cycle will take 0.5905 sec.

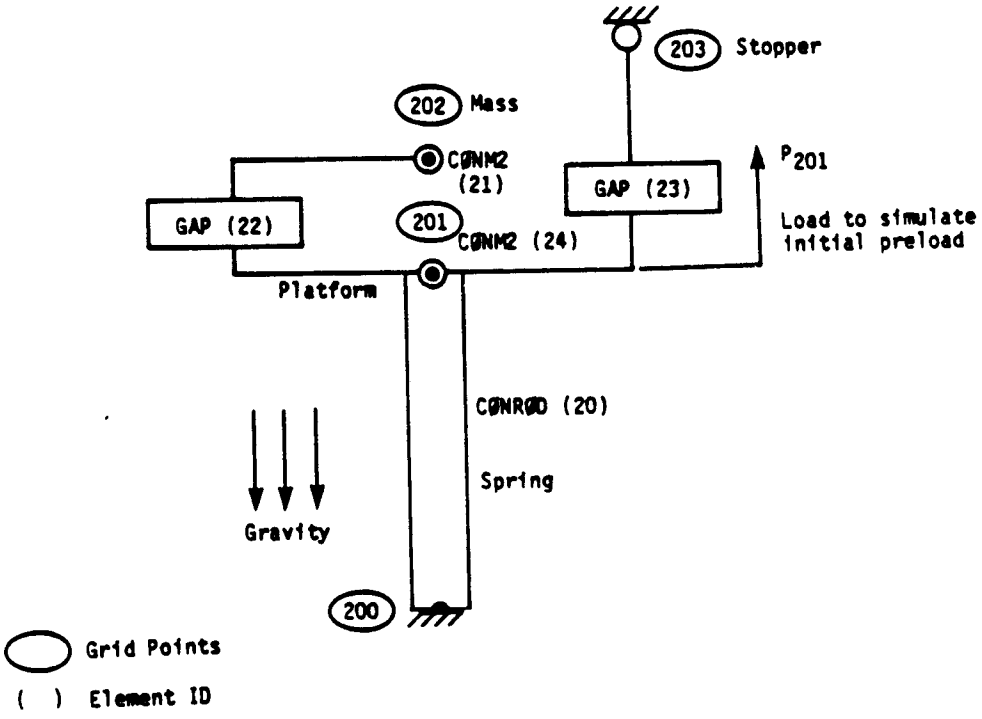

Figure 6. Symbolic MSC/NASTRAN Model

The MSC/NASTRAN model is depicted schematically in Figure 6. The spring is modeled with a CONROD element, for which the stiffness is given as $k = \frac{AE}{l}$, with A (area) = 1.0 in^2, E (Young's modulus) = 100 psi, and l (length) = 10 in. The mass is modeled as CONM2 21, which is connected to the platform (GRID 201) by GAP 22. The stopper is represented by a fixed point (GRID 203), to which the platform is connected by GAP 23. The base (GRID 200) is fixed to the ground. An initial displacement (4 inches) is simmulated by a step force (40 lbs) applied at GRID 201. The gravity field is applied by a GRAV entry. Static loads are converted to the dynamic loads using Bulk Data LSEQ and TLOAD2 with a Case Control command LOADSET. A small mass CONM2 24 (0.1 % of the mass block) is provided at the platform to suppress extraneous jittering. A small viscous damping (0.5 % at 31 rad/sec.) is introduced and adaptive time stepping is used.

The solution to the MSC/NASTRAN model is obtained by the nonlinear transient analysis method (SOL 99). The analysis started with initial Δt = 0.0025 sec. for the duration of 1 sec. GAP elements had the initial stiffness of 10^4 lb/in for the closed position with TMAX of 0.005 in. for adaptive adjustment. At the onset, the penalty value (K_a) of GAP 22 was adjusted to 10^5. The bisection was also activated by the adaptive time stepping during the initial phase. After the initial settlements, the automatic time stepping algorithm quadrupled the time step size. The stiffness matrix was updated three times due to GAP status changes in the vicinity of t = 0.035 sec., t = 0.545 sec. and t = 0.614 sec. The automatic time stepping algorithm caused the reduction of Δt to a half of the specified value (0.00125 sec.) while the platform was in motion around t = 0.58 sec.

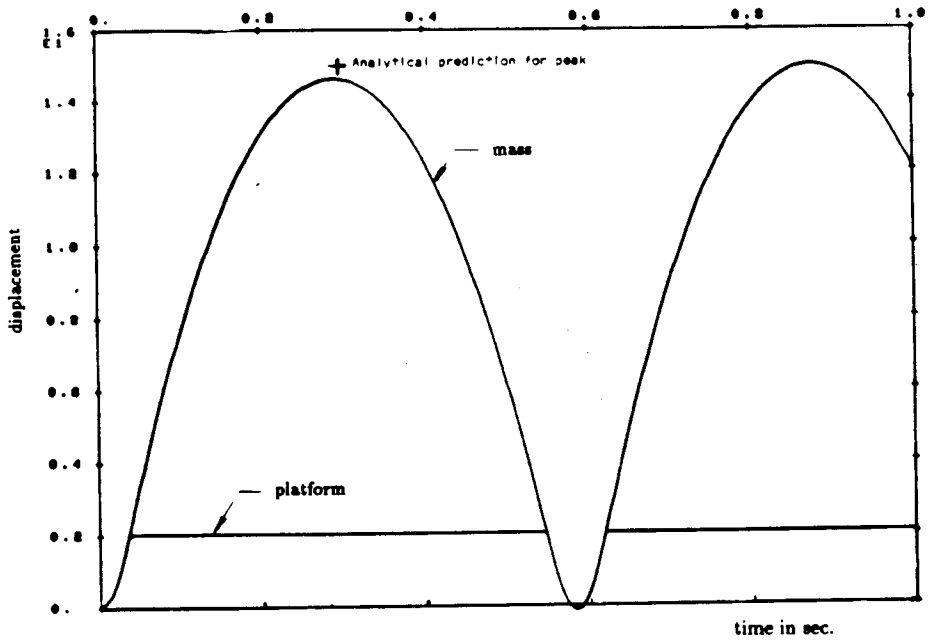

Figure 7. Displacement Response

The displacement response in Figure 7 shows a peak height of approximately 14.56 inches and the period of approximately 0.583 sec. Discrepancies between the MSC/NASTRAN solution and the analytical solution may be attributed to the following:

- Some momentum is dissipated due to the damping and the small mass introduced at the platform.
- The artificial stiffness introduced to the GAP elements changes the dynamic characteristics slightly.
- Due to the finite interval of the time increment, the time stepping scheme can not be synchronized exactly with the gap closing/opening.

In order to verify the adaptive penalty value adjustment algorithm, a parametric study is conducted with the penalty value (closed stiffness) of GAP 22. The value was varied from 10^3 to 10^7 with $TMAX = 0.005$. The effectiveness of adaptive penalty value adjustment is shown in Figure 8. Notice that penalty values were accepted in a wide range (10^4 to 10^6) by the adaptive adjustment scheme. A tighter tolerance ($TMAX = 0.001$) was also tested to examine its effect. Indeed, the penalty value was adjusted to the narrower range (10^5 to 10^6).

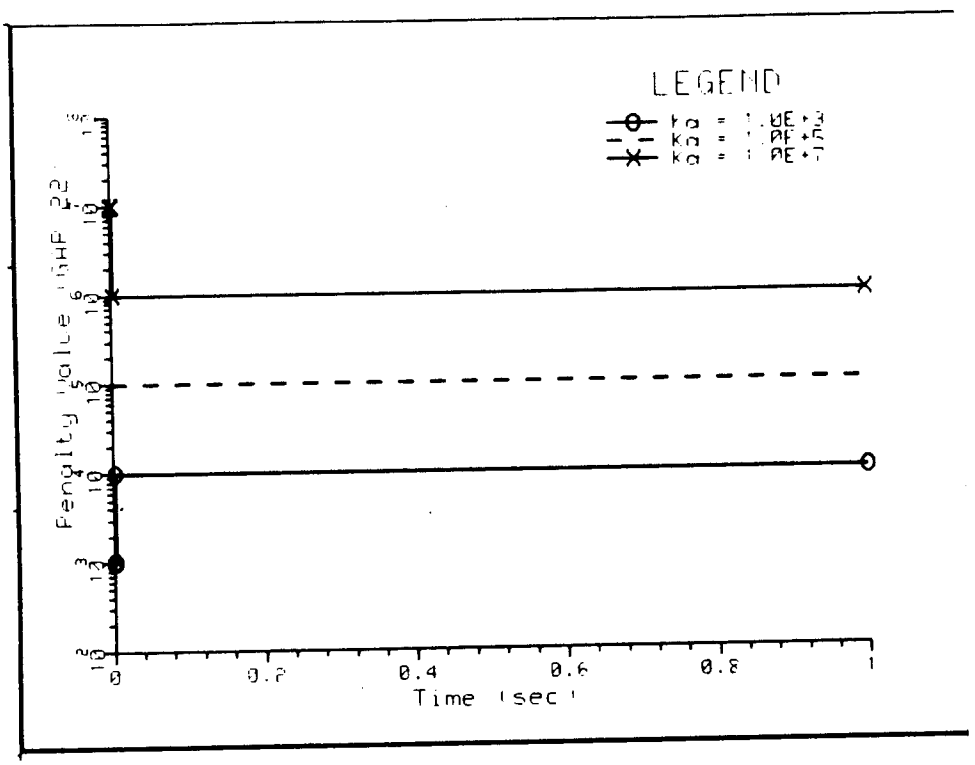

Figure 8. Adaptive Penalty Value Adjustment on GAP 22

VIBRATION WITH COULOMB DAMPING

A mass block (m) connected to a spring (k) is resting on a frictional surface as shown in Figure 9. The motion of the mass block is governed by

$$m\ddot{u} + ku = -F \qquad \text{for} \qquad \dot{u} > 0. \tag{29}$$

$$m\ddot{u} + ku = F \qquad \text{for} \qquad \dot{u} < 0.$$

where F is the friction force [12].

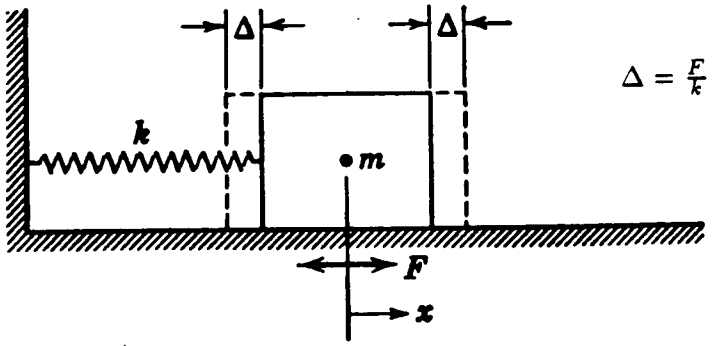

Figure 9. Physical Model for Vibration with Coulomb Damping [12]

Suppose the block is displaced by $u_0 >> F/k$ and released. The solution while $\dot{u} < 0$ is

$$u = \frac{F}{k} + (u_0 - \frac{F}{k}) \cos \omega t \tag{30}$$

where $\omega = \sqrt{k/m}$. The mass block comes to a stop ($\dot{u} = 0$) at $\omega t = \pi$. For $\pi \leq \omega t \leq 2\pi$ while $\dot{u} > 0$, the solution is

$$u = -\frac{F}{k} - (u_0 - 3\frac{F}{k}) \cos(\omega t - \pi) \tag{31}$$

It is noted that the acceleration ($\ddot{u}$) is discontinuous at $t = \frac{\pi}{\omega}, \frac{2\pi}{\omega}, \frac{3\pi}{\omega}, \cdots$, while the velocity is continuous. From the observation that $u = -(u_0 - 2F/k)$ at $t = \frac{\pi}{\omega}$, and $u = -(u_0 - 4F/k)$ at $t = \frac{2\pi}{\omega}$, the decay is a linear decrement at the rate of $4F/k$ per cycle until $\mid u_{max} \mid \leq \mid \frac{F}{k} \mid$.

The MSC/NASTRAN model uses a GAP element to simulate friction with $k_a = 10^6$, $k_t = 10^5$, $\mu_s = 0.3$ and $\mu_k = 0.2$. Let m (CONM2) be 100 kg in a gravity field of $1m/sec^2$, which gives rise to a normal force (F_N) of 100 N. A rod element is used to simulate an elastic spring with $k = 10^3$ N/m. The analysis is performed in three subcases using SOL 99. The first two subcases use PARAM, TSTATIC, 1 for static analyses, which apply the preloads (gravity and a horizontal force of P=220 N), resulting in an initial displacement

$$u_0 = \frac{1}{k}(P - \mu_k F_N) = 0.2$$

The third subcase uses PARAM, TSTATIC, 0 for dynamic response upon release of the load P. The natural frequency (ω) of the system is 3.1623 rad/sec and the period is 1.987 sec. After the first cycle, the amplitude decreases to

$$u_{max} = u_0 - 4\frac{\mu_k F_N}{k} = 0.2 - 4 \times 0.02 = 0.12$$

After two and a half cycles, the mass block is stagnated. Ideally, the mass block should come to a stop with a residual displacement due to friction. However, because of the shear stiffness (k_t) in the GAP element, the mass block oscillates at $\omega_r = \sqrt{k_t/m} = 31.623$ rad/sec. This effect is shown as ripples after two and a half cycles in Figure 10.

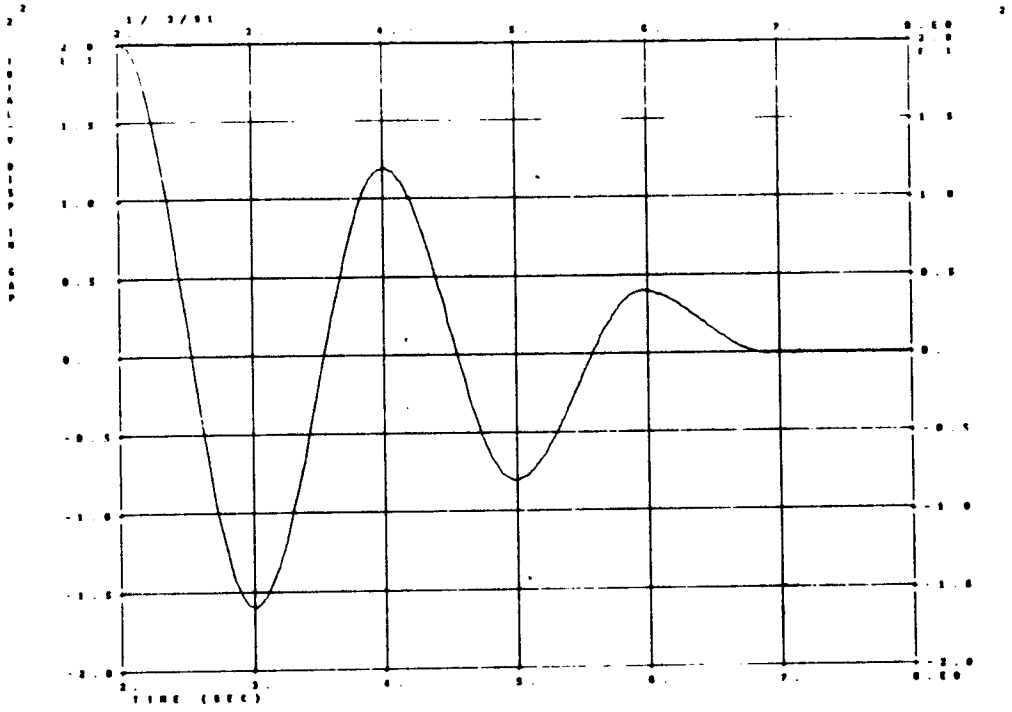

Figure 10. Horizontal Displacement Response

In order to examine the effects of the frictional force, the analysis is performed with some variations in the model. First, the mass (m) is increased to 366.7 kg and, in turn, the normal force (F_N) is increased to 366.7 N. Then the initial displacement (u_0) is decreased to 0.1467 and the natural frequency (ω) is reduced to 1.6514 rad/sec. In this case, the decay rate is such that the amplitude is reduced to zero in a half cycle ($\omega t = \pi$) as shown in Figure 11. This is analogous to the critically-damped case in viscous damping. If the friction coefficients are also increased ($\mu_s = 0.45$ and $\mu_k = 0.3$) and the horizontal applied force (P) is increased to 300 N, the initial displacement (u_0) becomes 0.19 m. The mass will come to rest when $\dot{u} = 0$, which

occurs at $t = \frac{\pi}{\omega} = 1.9$ sec. The residual displacement should have an asymptotic value of 0.03 from Eq. (30). As shown in Figure 11, this is analogous to the over-damped case in viscous damping.

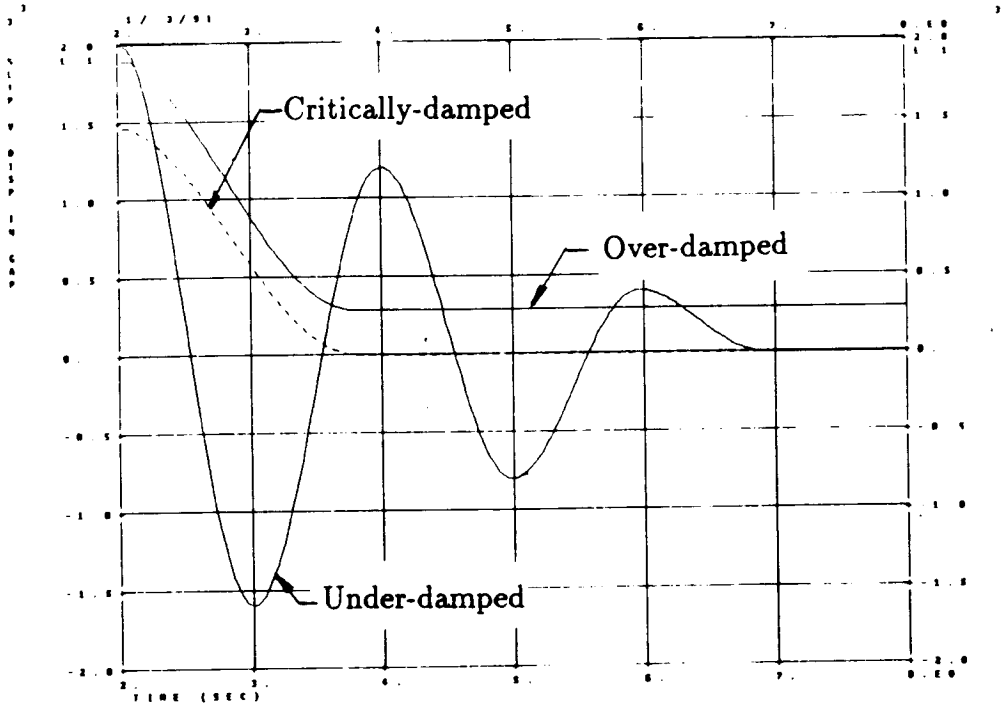

Figure 11. Comparison of Responses: Under-damped, Critically-damped, Over-damped

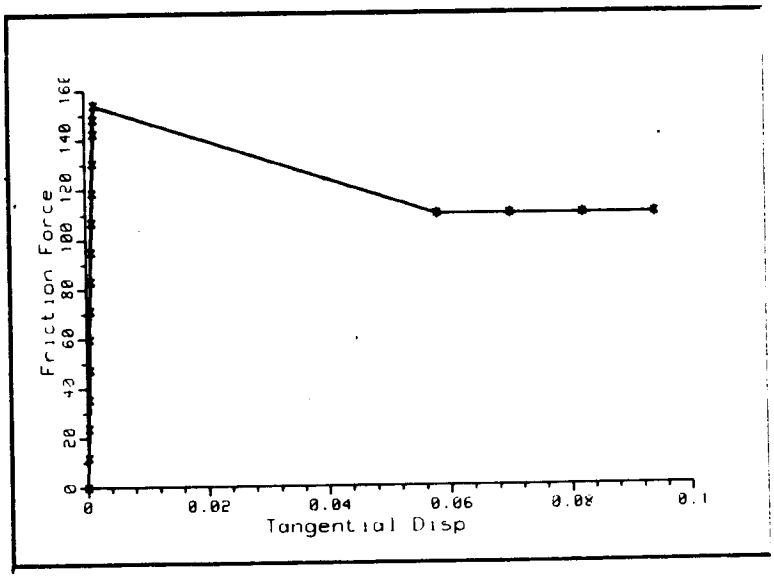

Figure 12. Horizontal Displacement during Static Loading

The effect of distinctive friction coefficients (static and kinetic) during the static loading is shown in Figure 12. For the over-damped case, the GAP will be sticking up to the friction force of 165 N, governed by μ_s. As the block starts to slip, the friction force is reduced to 110 N, complying with μ_k. It is noted that an excessive number of load steps was taken during the static loading in order to show the reduction in the frictional force at the stick/slip transition. Despite the excessive steps, the peak at 165 N is not shown due to the discrete load increment size.

HERTZIAN PROBLEM : CONTACT BETWEEN SPHERE AND RIGID PLANE

Mechanics of the frictionless contact between two elastic bodies were first solved by H. Hertz and published in 1881. Hertz presented solutions to a family of two-body contact problems with general curved surfaces for the loading normal to the surface. Stresses at the contact area depend on the deformation of the bodies in contact. Typical examples are ball and roller bearings, gears, cams, and rolling wheels. Hertz's analysis revealed that the pressure distribution on the contact surface between two curved bodies is represented by a semiellipsoid constructed on the surface of contact.

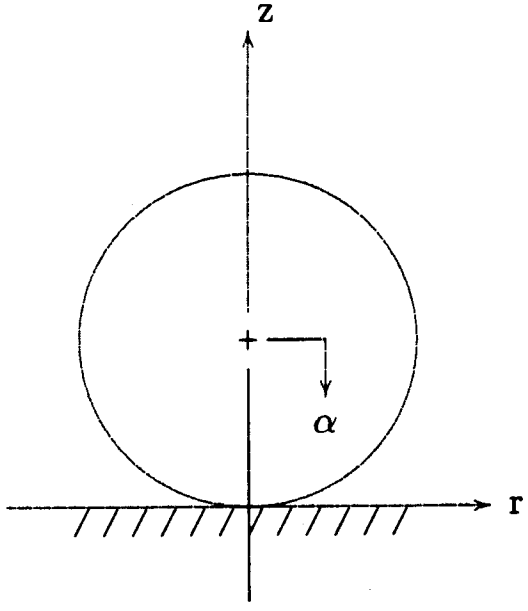

Figure 13. Contact between Elastic Sphere and Rigid Plane

Let us confine our discussion to the contact of an elastic sphere with a rigid plane as shown in Figure 13. The hemispherical pressure distribution on the surface of contact with a radius a gives the maximum pressure (q_0) at the center by

$$q_0 = \frac{3P}{2\pi a^2} \tag{32}$$

where P is the total compressive force. The solution for two balls in contact with radii R_1 and R_2 is given [13] with the radius of contact area as follows:

$$a = \left[\frac{3\pi}{4}\frac{P(k_1+k_2)R_1R_2}{R_1+R_2}\right]^{1/3} \tag{33}$$

and for the rigid body motion (or approach distance)

$$\alpha = \left[\frac{9\pi^2}{16}\frac{P^2(k_1+k_2)^2(R_1+R_2)}{R_1R_2}\right]^{1/3} \tag{34}$$

with

$$k_1 = \frac{1-\nu_1^2}{\pi E_1} \qquad \text{and} \qquad k_2 = \frac{1-\nu_2^2}{\pi E_2}$$

for two balls (1 and 2) with different Young's moduli and Poisson's ratios, respectively. For the contact of an elastic sphere with a rigid flat plane, Eqs. (33) and (34) are reduced with $R_2 = \infty$ and $E_2 = \infty$ to

$$a = \left[\frac{3(1-\nu^2)}{4E}PR\right]^{1/3} = \sqrt{R\alpha} \tag{33a}$$

and

$$\alpha = \left[\frac{9}{16}\frac{P^2}{R}\frac{(1-\nu^2)^2}{E^2}\right]^{1/3} \tag{34a}$$

where α is identical to the displacement of points on the sphere remote from the deformed area.

Stresses at the center of the contact surface are given by

$$\sigma_r = \sigma_\theta = \frac{1}{2}(1+2\nu)\sigma_z \qquad \text{and} \qquad \sigma_z = -q_0$$

The maximum shear stress occurs on the z-axis at a distance of $0.47a$ below the surface of contact, given as

$$\tau_{rz} = \tau_{\theta z} = 0.31q_0$$

The maximum tensile stress occurs at the circular contact boundary, given as

$$\sigma_r = \frac{1-2\nu}{3}q_0$$

At this boundary, the circumferential stress (σ_θ) is compressive with the same magnitude as σ_r, which represents a pure shear stress state.

For the static analysis, a symmetric half of a 10 degree sector of the sphere is modeled by HEXA and PENTA elements with axisymmetric boundary conditions as shown in Figure 14. Contact with a rigid plane is simulated by adaptive GAP elements. Uniform vertical displacement of the symmetric plane is maintained by tying the vertical displacements of all the nodes

on the top plane (loading plane) by MPC relations to the one at the centerline (z-axis), on which 1/36 of the total compressive force is applied.

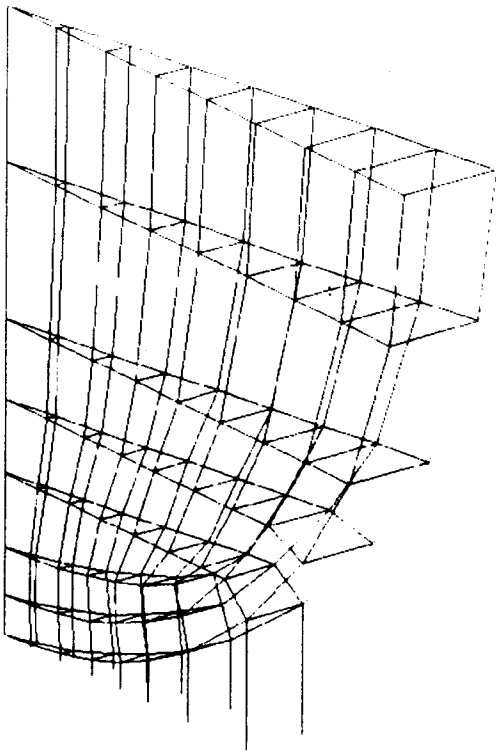

$R = 8.0$ in.
$E = 1000$ psi.
$\nu = 0.3$

Figure 14. MSC/NASTRAN Model for Static Analysis

The static analysis was performed in 20 increments up to the maximum loading ($P = 2160$). The analysis ran to completion in 27 iterations with four GAP induced stiffness updates. The deformed shape at the maximum loading is shown in Figure 15 in comparison with the undeformed model. Two additional cases were analyzed: one with geometric nonlinearity (PARAM, LGDISP) and the other with friction ($\mu_s = 0.3$ and $\mu_k = 0.2$). Deformed shapes for other cases were not discernible from the one in Figure 15. All cases ran to completion without requiring any user intervention. In the frictional case, however, bisections were activated three times during the initial phase, and 30 incremental steps were required.

The radius of contact surface and the approach distance (vertical displacement at the loading plane) are plotted as functions of the total force (P) in Figure 16, which shows the MSC/NASTRAN solution in comparison with the Hertz solution. Notice that the effects of friction and geometric nonlinearity are gradually manifested as the load increases. It is noted that the frictional case appears more accurate at the initial stage. This is because the frictional case took much smaller increments due to bisections during the initial phase, and the point of contact could be more closely predicted.

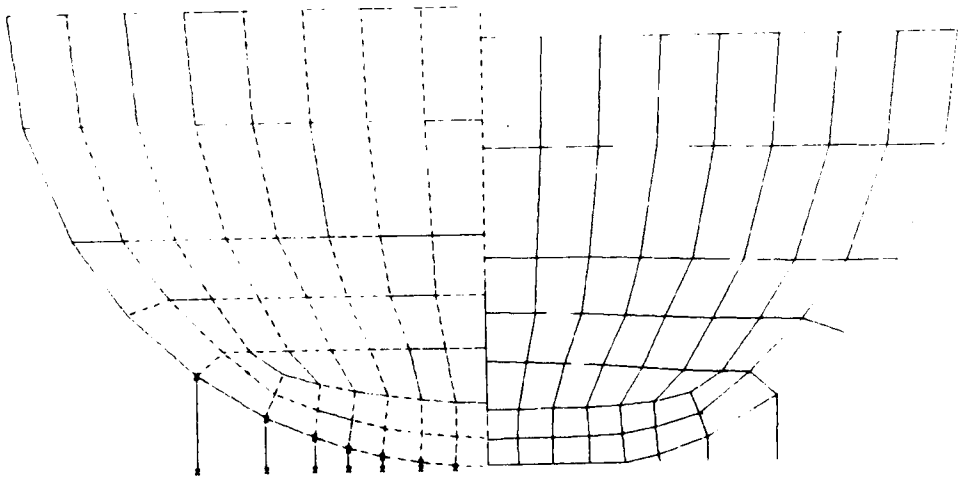

Figure 15. Undeformed Shape vs. Deformed Shape at $P = 2160$

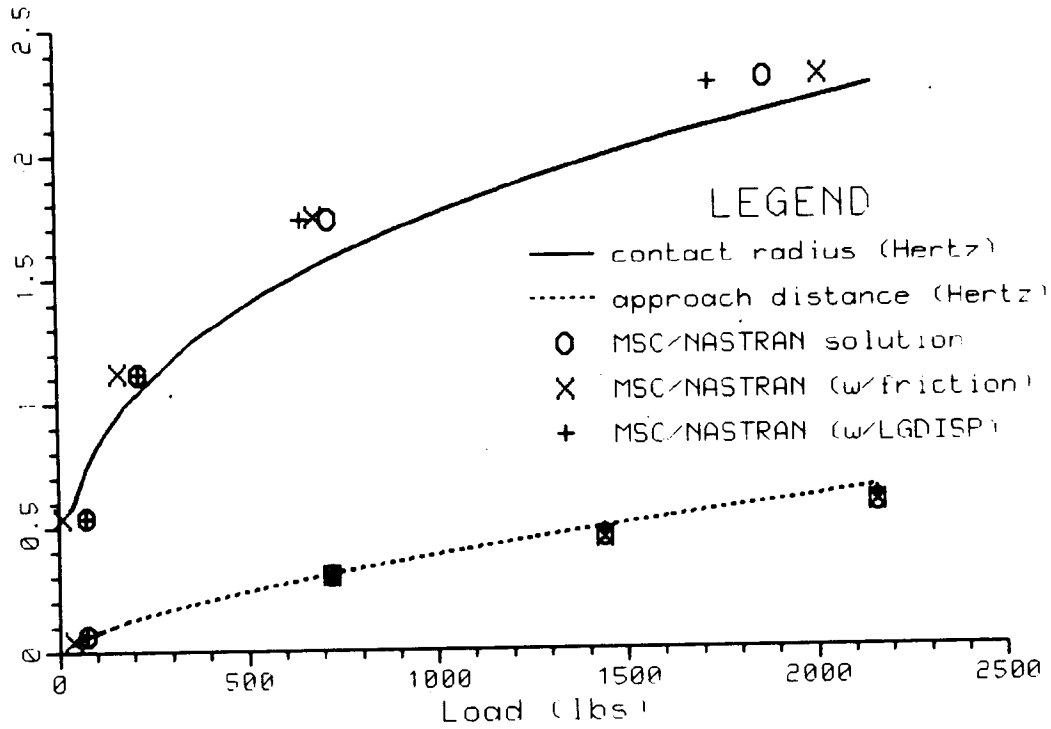

Figure 16. Contact Radius & Approach vs. Total Force in Static Analysis

DYNAMIC CASE : IMPACT OF A SPHERE TO RIGID PLANE

The hertzian problem shown in Figure 13 is considered for dynamic response. In the impact of an elastic sphere with the rigid plane, the duration of contact is very long compared to the period of lowest mode of vibration in the sphere. Vibrations and the stress wave can therefore be neglected, and the statical solutions in Eqs. (33a) and (34a) are assumed to be valid during impact [13]. The applied force P can be obtained from

$$m\dot{v} = m\ddot{\alpha} = -P$$

where m and v are the mass and the velocity of the sphere, respectively. Introducing a notation

$$n = P\alpha^{-3/2} = \frac{4}{3}\frac{ER^{1/2}}{(1-\nu^2)}$$

the acceleration of approach becomes

$$\ddot{\alpha} = -\frac{n}{m}\alpha^{3/2}$$

from which

$$\frac{1}{2}(\dot{\alpha}^2 - v_0^2) = -\frac{2}{5}\frac{n}{m}\alpha^{5/2} \tag{35}$$

where v_0 is the velocity of the sphere at the beginning of impact.

The value of the maximum compressive force is obtained by

$$P_{max} = n[\alpha_{max}]^{3/2} \tag{36}$$

where α_{max} at the maximum compression can be found by substituting $\dot{\alpha} = 0$ into Eq (35), resulting in

$$\alpha_{max} = \left[\frac{5m}{4n}v_0^2\right]^{2/5} = \left[\frac{5}{4}\pi\rho\frac{1-\nu^2}{E}v_0^2\right]^{2/5} R \tag{37}$$

where ρ is the mass density of the sphere. The duration of impact is given by

$$t = 2.94\frac{\alpha_{max}}{v_0} = 2.94\left[\frac{5}{4}\pi\rho\frac{1-\nu^2}{E}\right]^{2/5} Rv_0^{-1/5} \tag{38}$$

For the impact analysis, a 10 degree sector of the sphere is modeled by HEXA and PENTA elements with axisymmetric boundary conditions as shown in Figure 17. Contact with a rigid plane is simulated by adaptive GAP elements. The initial velocity of 10 in/sec. is specified for the sphere at the beginning of the impact. The analysis started with the initial time step size of 1 $m$sec. and progressed to completion without any difficulty. The adaptive time stepping algorithm adjusted Δt to 2 and 4 $m$sec. during the initial stage. The bisection was activated during the maximum impact to adjust Δt to 0.25 $m$sec. In the mean time the GAP induced stiffness updates were activated (a total of 15 times) when GAPs were closing. After the peak

impact, the time step size fluctuated between 0.25 $m$sec. and 4.0 $m$sec. due to thrashing of bisection and automatic adjustment, which seems to have been caused by opening GAPs and the algorithm that did not activate the stiffness update.

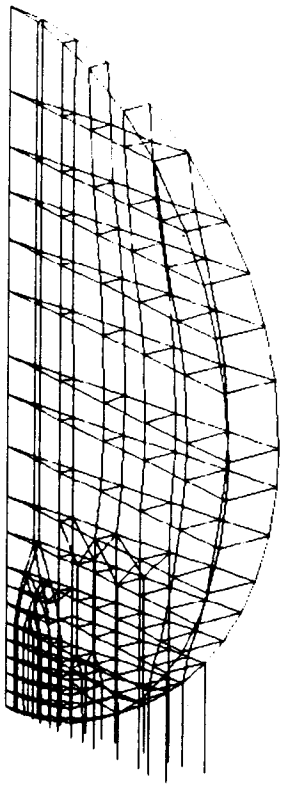

$R = 5.0$ in.
$E = 1000$ psi.
$\nu = 0.3$
$\rho = 0.01$ lb-sec^2/in^4

$v_0 = 10.$ in/sec.

Figure 17. MSC/NASTRAN Model for Dynamic Analysis

According to Eqs. (36) and (37), the maximum compression force (P_{max}) is 1246.5 lbs, which occurs when the approach distance (α_{max}) reaches 0.5251. MSC/NASTRAN analysis shows $P_{max} \simeq 1440$ and $\alpha_{max} \simeq 0.53$ as shown in Figures 18 and 19, respectively. As exhibited by jagged responses in Figure 18, some effect of the stress wave is manifested when GAPs are opening. The maximum indentation occurs in the vicinity of $t = 0.072$ sec. with the contact radius of approximately 1.71 while Eq. (33a) predicts 1.62. The duration of impact is 0.1544 sec. from Eq. (38). MSC/NASTRAN analysis as shown in Figure 18 indicates that the duration is around 0.143 sec. Small discrepancies are attributed to the discrete contact rather than continuous contact due to the discreteness in space and time. Figure 20 shows snap shots of the deformed configuration at time 0.051 sec., 0.072 sec. and 0.2 sec.

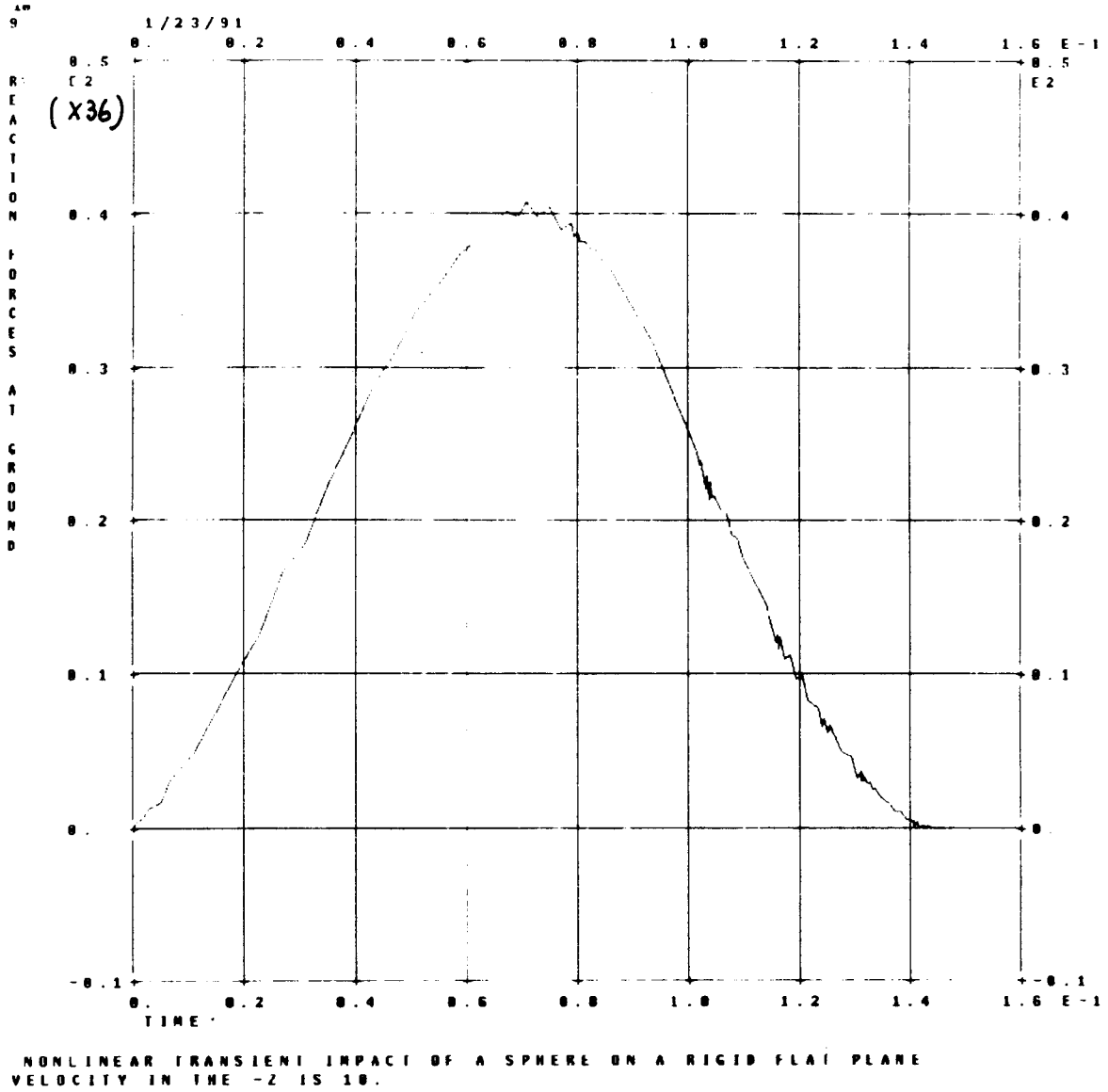

Figure 18. Reaction Force vs. Time

Curves in the order of
Near contact point
Center point on mid-plane
Point at the top

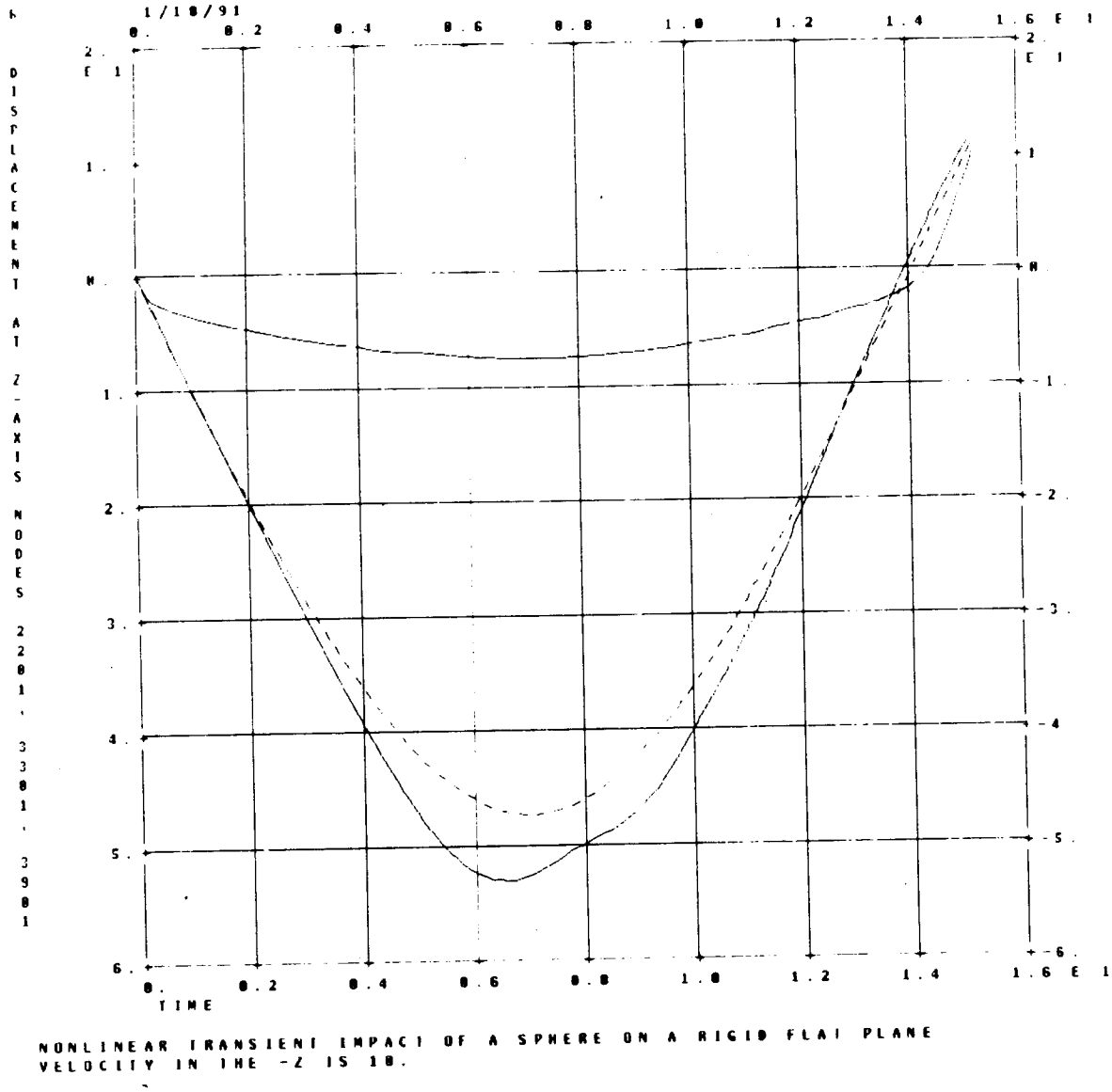

Figure 19. Vertical Displacement Response at Select Points on Center Line

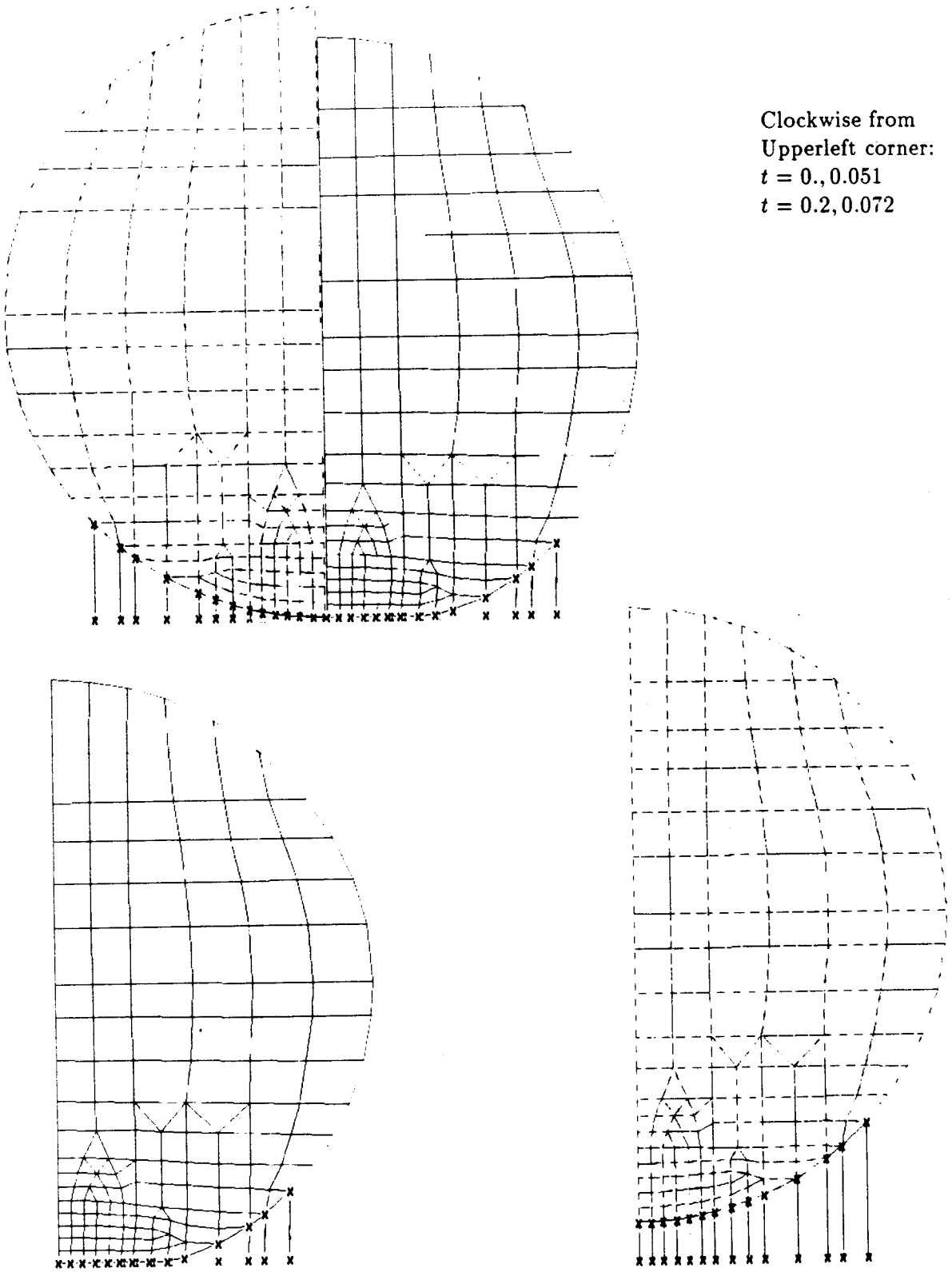

Clockwise from
Upperleft corner:
$t = 0., 0.051$
$t = 0.2, 0.072$

Figure 20. Snap Shots at t=0., 0.051, 0.072 and 0.2 sec.

VIII. CONCLUDING REMARKS

The most crucial task in using the GAP element was to determine proper penalty values, which dictates the accuracy, efficiency and the effectiveness of the analysis. Penalty values should be chosen as large as possible for solution accuracy but as small as possible for solution efficiency. The recommended value for the penalty stiffness is 1000 times the stiffness of the adjacent structure, which will produce an error of 0.1%. Even with the advanced knowledge of the structural characteristics of the contact region, user specification of the penalty stiffness is merely an educated guess. This guess has to be a conservative one at the expense of the computational efficiency, because the proper value varies throughout the analysis.

The main goal of the self-adaptive method is to relieve users from the chores and uncertainties of guessing or trial-and-error searches. By achieving this goal, an optimum algorithm design is automatically attained for efficiency as well as for solution accuracy. A self-adaptive algorithm has been proven effective and efficient for nonlinar analysis in MSC/NASTRAN. The primary virtue of the adaptive method, however, is not the computing efficiency but the overall engineering efficiency. This is because the adaptability makes it possible to obtain the solution at the very first trial.

The adaptive GAP element, in concert with adaptive solution methods [10,14], made it possible to maintain an acceptable accuracy while maintaining the solution efficiency without user intervention throughout the dynamic environment of nonlinear computation. The negative impression of the old GAP element based on non-adaptive algorithm should be erased. The applicability of the present algorithm is deemed viable to simulation of surface contacts with friction.

ACKNOWLEDGEMENTS:

Authors wish to thank Ms. A. Raiten for her assistance in modeling and analysis.

REFERENCES

1. T. J. R. Hughes, R. L. Taylor, J. L. Sackman, A. Curnier and W. Kanoknukulchai, "A Finite Element Method for a Class of Contact Problems," *Comp. Meth. in Appl. Mech. Eng.* , Vol. 8, pp. 249-279, 1976.
2. K. J. Bathe and A. Chaudhary, "A Solution Method for Planar and Axisymmetric Contact Problems," *Int. J. Num. Meth. Eng.*, 21, pp. 65-88, 1985.
3. A. B. Chaudhary and K. J. Bathe, "A Solution Method for Static and Dynamic Analysis of Three-dimensional Contact Problems with Friction," *Computers & Structures*, Vol. 24, No. 6, pp. 855-873, 1986.
4. J. C. Simo, P. Wriggers and R. L. Taylor, "A Perturbed Lagrangian Formulation for the Finite Element Solution of Contact Problems," *Comp. Meth. Appl. Mech. Eng.*, 50, pp. 163-180, 1985.

5. J. W. Ju and R. L. Taylor, "A Perturbed Lagrangian Formulation for the Finite Element Solution of Nonlinear Frictional Contact Problems," *J. Theo. and Appl. Mech.*, 7, 1988.

6. J. A. Landers and R. L. Taylor, "An Augmented Lagrangian Formulation for the Finite Element Solution of Contact Problems," UCB/SESM-85/09, Dept. of Civil Eng., University of California, Berkeley, 1985.

7. L. T. Campos, J. T. Oden, and N. Kikuchi, "A Numerical Analysis of a Class of Contact Problems with Friction in Elastostatics," *Comp. Meth. Appl. Mech. Eng.* , 34, pp. 821-845, 1982.

8. J. H. Cheng and N. Kikuchi, "An analysis of Metal Forming Processes using Large Deformation Elastic-Plastic Formulations," *Comp. Meth. Appl. Mech. Eng.*, Vol. 49, pp. 71-108, 1985.

9. S. H. Lee, "Some Salient Considerations for Computational Procedure in Elasto-plastic Material Model," Proc. of MSC/NASTRAN Users Conference, Seoul, Korea, October 22-23, 1990.

10. S. H. Lee and S. S. Hsieh, "Expedient Implicit Integration with Adaptive Time Stepping Algorithm for Nonlinear Transient Analysis," *Comp. Meth. Appl. Mech. Eng.* , Vol. 81, No. 22, pp. 151-172, 1990.

11. R. F. Steidel, Jr., *An Introduction to Mechanical Vibrations*, John Wiley & Sons, New York, 1971.

12. S. Timoshenko, D. H. Young and W. Weaver, Jr., *Vibration Problems in Engineering*, Fourth Edition, pp. 198–199, John Wiley & Sons, New York, 1974.

13. S. Timoshenko and J. N. Goodier, *Theory of Elasticity*, Third Edition, pp. 409–421, McGraw-Hill, New York, 1970.

14. S. H. Lee, S. S. Hsieh and T. L. Bock, "Adaptive Arc-Length Methods in MSC/NASTRAN," proceedings of 1990 MSC World Users Conference, 5/1-22, Los Angeles, March 28, 1990.